A Variable Stiffness Soft Actuator for Hand Rehabilitation

Muhammad H. Alvi, Jiaming Fu, Brittany A. Newell, and Dongming Gan, *Member, IEEE*

***Abstract*— Stroke patients have a pressing demand for innovative hand rehabilitation devices with multiple finger joint positions. In this research, a novel soft variable stiffness actuator is proposed for alternative hand rehabilitation therapies. The design allows targeted stiffness modifications above specific joints, enabling a range of motions from a simple actuation source, supplemented by a smaller actuator determining internal stiffness. Four configurations were tested, adjusting stiffness regions within the actuator. Initial testing employed Finite Element Analysis simulations with hyper-elastic non-linear material settings, predicting actuator behavior under varying pressure. Comparison of simulation and experimental results, despite differing actuation pressure due to air leaks, revealed an acceptable replication of Finite Element Analysis simulations, with minor differences in tip trajectory. Validation involved testing a single prototype, laying the groundwork for a new form of variable stiffness actuator. The results indicate that the proposed soft variable stiffness actuator can achieve diverse hand rehabilitation guidance postures under the desired force, making it applicable to next-generation hand rehabilitation gloves and other devices.**

I. Introduction

Over the past decades, the number of stroke patients worldwide has gradually increased. Stroke is a neurological disorder with complex connections to risk factors such as hypertension, diabetes, hyperlipidemia, heart disease, and obesity [1]. Consequently, these conditions compromise various physiological functions in individuals [2,3], with impaired hand mobility significantly affecting the overall convenience of daily life. Fortunately, patients with impaired hand functionality can engage in continuous passive motion exercises to partially restore hand mobility, including repetitive tasks such as grasping and opposition motion [4]. These exercises can be offered by utilizing assistive or rehabilitation robots. Currently, several rehabilitation technologies, including training equipment and assistive devices, have been implemented. The rise in need for these robots has created a market worth USD 500 million with an estimated 22.6% compounded annual growth rate (CAGR) until 2026 [5]. To date, numerous research endeavors have focused on the development of robotic devices for upper limb training in stroke patients [6], encompassing various wearable hand-assistive devices. Notably, lightweight, comfortable, and effective exoskeletons, as well as soft robotic gloves designed for post-stroke hand rehabilitation, have received positive feedback from patients [6]. However, the common feature amongst all these rehabilitation robots is that they offer a single therapy of a simple open-close motion.

* This research work is supported by the National Science Foundation (NSF) grant under FRR-2131711.

M. H. Alvi is with Purdue University School of Engineering Technology, M.S. in Engineering Technology, West Lafayette, IN 47907 (alvim@purdue.edu).

J. Fu is with Purdue University School of Engineering Technology, PhD in Engineering Technology, West Lafayette, IN 47907 (fu330@purdue.edu).

B. A. Newell is with the School of Engineering Technology, Purdue University, West Lafayette, IN 47907 (bnewell1@purdue.edu).

D. Gan is the corresponding Author. He is with the School of Engineering Technology, Purdue University, West Lafayette, IN 47907 (dgan@purdue.edu).

A. Conventional and Alternative Rehabilitation Therapy

Most of the currently available rehabilitation robots applied in the market offer a singular therapy focused on opening and closing positions. These therapies are conventional and involve repetitive hand movements in gripping motions, rather than accommodating multiple hand positions. When therapies requiring different hand positions are needed, they often prove challenging to implement or necessitate the replacement of various equipment versions, causing inconvenience for patients. Research by Friedman et al. indicates that the utilization of alternative hand rehabilitation therapies, which involve complex finger movements, can enhance hand functionality when compared to traditional therapies [7].

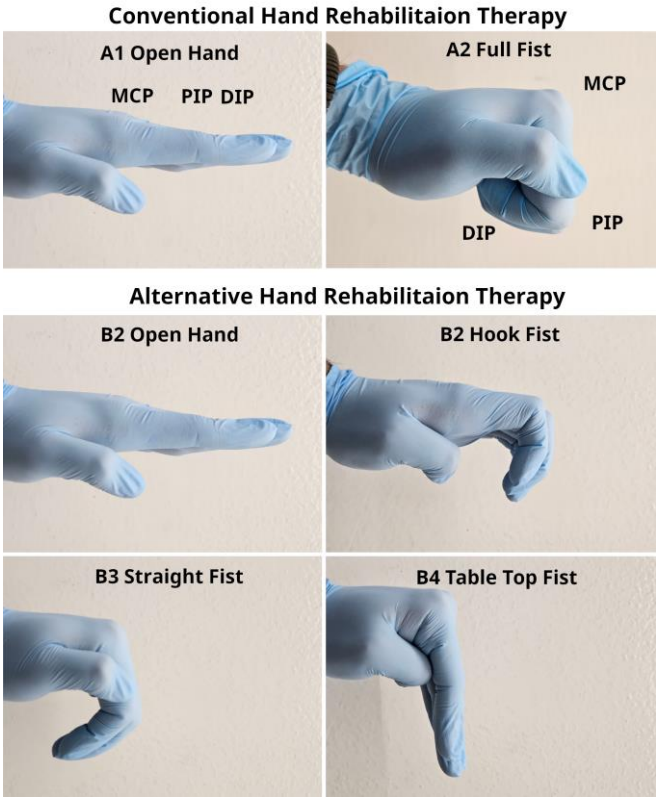

Figure 1. Hand rehabilitation therapies.

The alternative therapies recommend incorporating high-frequency complex finger movements to improve the partial restoration of hand mobility in patients [7]. The motions can be defined as manipulating the individual Metacarpal-phalangeal (MCP), Proximal interphalangeal (PIP), and Distal interphalangeal (DIP) joints on the four main fingers on the hand as shown in Fig. 1. Rehabilitation therapies involving single joint-blocking orthosis movements inhibit the movement of a selected joint on the finger and activate the remaining ones. The alternate hand rehabilitation therapies provide overall better hand functional outcomes with less pain over the course of the therapy [8]. Moreover, single joint-blocking orthosis movements are also essential for stopping the formation of tendon adhesions within the finger joints and preserving hand mobility [9]. Fig. 1 shows a set of proposed alternate therapies against conventional hand rehabilitation therapies. The conventional therapies consist of open and closed fists while the alternate therapy adds the straight fist, the hook fist, and the table-top fist to the therapy. The alternate therapy proposed blocks a single joint in the finger while actuating the remaining joints.

B. *Related Works*

In order to implement the alternative therapies, researchers have proposed several soft wearable exoskeletons designed for hand rehabilitation. For instance, [10] introduces a soft wearable exoskeleton composed of a glove embedded with pneumatic actuators of variable stiffness, capable of conforming to the finger profile during actuation. Similarly, [11] develops a Variable Stiffness Soft Robotic Glove with a multi-stage articulated elastomer providing stiffness adjustment to accommodate varying joint resistance. However, it is noteworthy that these soft wearable exoskeletons generally exhibit limitations in providing a substantial ratio of stiffness variation.

Researchers have also explored alternative variable stiffness mechanisms [12], which hold potential for applications in hand rehabilitation. [13] proposes a continuum robot with a variable stiffness mechanism powered by a set of embedded Shape Memory Alloy (SMA) springs. While its branches can bend to adapt to finger shapes, it may require extended cooling time. [14] demonstrates soft–rigid tendon-driven modular grippers using interpenetrating phase composite materials, showcasing excellent shape adaptability, but with limited ability to achieve significant stiffness changes. On a different note, [15] introduces a discrete variable stiffness gripper based on the fin ray structure, capable of achieving discrete stiffness changes, but occupying a substantial amount of space with its stiffness adjustment mechanism. Additionally, [16] establishes a variable stiffness gripper based on layer jamming, capable of increasing payload but facing challenges in easy repositioning. In [17], a gripper utilizing pneumatic pouch actuators to adjust adaptable flaps on flexure hinges is illustrated. While it facilitates stiffness adjustment in multiple joints, it is noted for its insufficient ratio of stiffness variation. [18] introduces a continuous variable stiffness robotic gripper with the advantage of rapid online stiffness adjustment but is limited to single-joint applications.

C. *Proposed Solution*

In contrast to these approaches, this paper proposes the design and development of a novel variable stiffness soft actuator (VSSA) that can manipulate the stiffness of selective regions within the actuator. The VSSA is a modification of a soft robot actuator with a slot chamber underneath the base of the actuator. The slot contains a stiffness beam that is positioned at a desired location, which changes the local stiffness within the region. The VSSA can be used on hand rehabilitation gloves that will implement alternative rehabilitation therapies by manipulating the stiffness of the region above the individual finger joints. The varying stiffness of the region above the joints allows the actuator to only bend in desired regions. The feature allows the fingers to be bent as shown in the alternative therapies section of Fig. 1. Soft actuator designs used in conventional hand rehabilitation therapies have a single degree of freedom (DOF), whereas introducing the design of the VSSA allows for varying DOF within the actuator enabling alternative multi-joint control of fingers in hand rehabilitation therapies. The image in Fig. 2 shows how the VSSA can be applied in rehabilitation therapies.

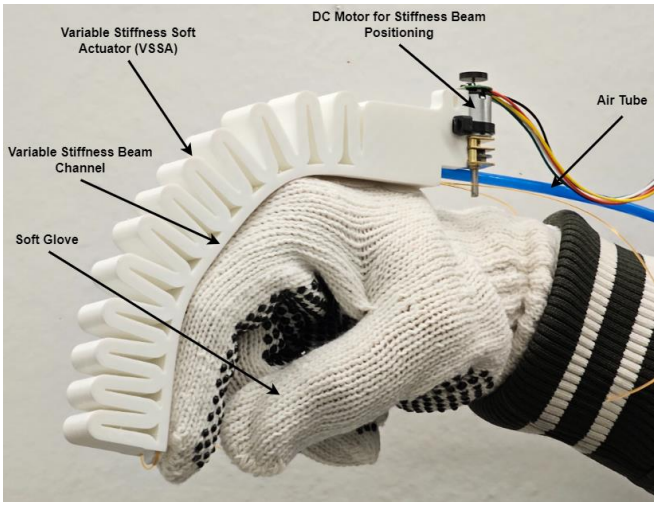

Figure 2. VSSA concept.

The topics in this paper cover the characteristics of the material used to develop the VSSA. The design details of integrating variable stiffness elements in soft actuators are also further discussed along with the manufacturing process used to fabricate the VSSA in Section II. Additionally, in Section III, the simulation setup and process are discussed, and the retrieved results are compared against experimental data to measure the performance of the VSSA design. Section IV discusses challenges and limitations. Conclusions are drawn in Section V.

II. Material and Design

The VSSA was constructed using additive manufacturing technology of 3D printing. The material used was the "Filaflex TPU" with a shore hardness of 60A. Thermoplastic Polyurethane (TPU) is a flexible material that can be used for 3D printed applications. The design is fabricated using a modified 3D printer extruder head which has dual contact regions on the filament extruder head, allowing the material to be pulled uniformly. The uniform forces applied on the

flexible material prevent it from jamming the extruder head during the printing process.

A. Material Characteristics

The flexible 3D printing filament from Filaflex is formed from a class of material polymers from polyurethane. The material is naturally a high-elasticity plastic which allows it to be deformed in a manner such as bending and flexing easily [19]. The behavior of the material can be labeled as a hyper-elastic material which is used in the study of the paper.

Creating a functional design to perform accurate simulations of the actuator design requires the material's stress-strain curve to be mapped in the simulation software. A uniaxial tensile test was conducted to map the stress-strain curve of the material selected for the VSSA. Four samples of ASTM D638 type IV as shown in Fig. 3 were used for the test [20] and fabricated using 3D printing. The test specimens were printed at a 100% infill with the print line orientation set to the longitudinal axis of the test [21]. The tests were conducted on the Universal Force Testing Systems (Instron 34SC-5) with a constant extension rate of 50 mm/min.

Figure 3. ASTM D683 Type IV sample with longitudinal print orientation.

The resulting data points collected from the experiments were combined and an average value of the stress-strain curve for the model was created. The material density of the Filaflex TPU was retrieved as per the datasheet of the material to be 1.07 g/cm^3 [22]. The average of the four stress-strain graphs of the material were then inserted into the simulation software. The simulation software used for the study was ANSYS Workbench. The material's stress-strain characteristics were subsequently analyzed by employing a well-established hyper-elastic model, specifically the Mooney-Rivlin model, for deformation prediction [19]. Fig. 4 visually represents the curve fitting process for the Mooney-Rivlin second order model, based on the experimental data. In this depiction, the blue line corresponds to the uniaxial test data points, while the red line signifies the curve fit achieved using the Mooney-Rivlin 2nd order model.

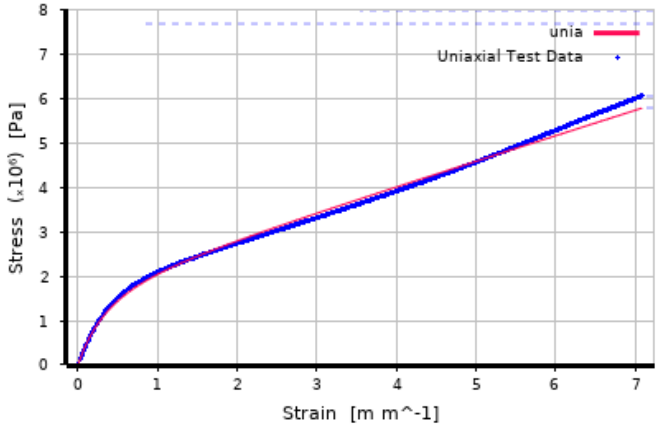

Figure 4. TPU Stress-strain curve with Mooney-Rivlin 2nd order curve fit.

The strain energy equation representing this model is expressed as Equation (1):

$$W = C_{10}\,(I_1 - 3) + C_{01}\,(I_2 - 3) + \frac{1}{D_1}\,(J-1)^2 \qquad (1)$$

Here, the parameters C_{10} and C_{01} denote material-specific constants. The first deviatoric strain invariant is I_1 and the second deviatoric strain invariant is I_2 while the incompressibility parameter is indicated by D_1. The hyper-elastic material used was assumed to be incompressible, hence, the result from only applying a uniaxial test data set to the Mooney-Rivlin model results in a value of zero for the D_1 parameter. In the case of incompressible materials, the variable J represents the elastic deformation gradient, and it is constrained to one due to the incompressibility of such materials. Consequently, in the last segment of the equation, this term becomes zero. This mathematical adjustment reflects the characteristic of incompressible materials, where volumetric changes are limited, rendering this portion of the equation negligible in the computation of strain energy. The two-parameter incompressible Mooney-Rivlin material model is then employed to characterize the local behavior of the TPU hyper-elastic material [23]. The parameters retrieved from the Mooney-Rivlin second order curve fit are displayed in Table I below.

TABLE I. Hyper-elastic material properties.

Coefficient	Value	Unit
Material Constant C01	0.59641	MPa
Material Constant C10	0.28548	MPa
Incompressibility Parameter D1	0	MPa^{-1}
Density	1.07	g/cm^3

B. Design of the VSSA

The VSSA is based on a sinusoidal wave-bending actuator design. The actuator has a hollow internal cavity with thin walls. The walls of the actuator were kept 1.2mm thick. The sinusoidal wave pattern extends the actuator linearly when the internal cavity is pressurized. To ensure that the actuator bends when the chamber is pressurized, a thin beam is attached to the desired bending side which constricts the expansion of the actuator in that direction. The initiation of bending motion is accomplished by applying pneumatic pressure to the internal expansion chambers of the VSSA. The resultant pressurization causes the unfolding of folds in the expansion chamber, setting in motion an asymmetrical bending response. This distinct asymmetry is deliberately introduced through the incorporation of a constriction beam exclusively on one side of the actuator. The strategic placement of this layer contributes to the controlled and directional bending behavior, a crucial aspect in tailoring the actuator's mechanical response for specific applications. This design choice allows for precise manipulation of the bending characteristics, enhancing the versatility and adaptability of the pneumatic actuator in practical scenarios. [24].

Until now, the actuator design has not been very unique and has been thoroughly developed in the area of soft bending actuators. The key feature of the VSSA is that it consists of a hollow slider chamber under the constriction beam of the actuator. The hollow chamber contains a rigid material (3D

printed PLA or Steel) stiffness beam which can be placed in any desired location under the actuator. The stiffness beam is attached to the hollow chamber through a slider contact joint under the pneumatically actuated sinusoidal wave-bending feature. The position of the beam is controlled through a closed-loop cable and pulley system, actuated from a small DC motor. The DC motor consists of an encoder which is used to determine the position of the stiffness beam in the VSSA based on the diameter of the pulley and the encoder value. The DC motor is used as a low-power actuator that quickly modifies the position of the stiffness beam in the slider chamber which enables reconfigurable regions of varying stiffness within the actuator. Next to the slider chamber, another small tube feature is present in the design that guides the cable back to the pulley on the actuator. The tube feature enables the cable-pulley to be a closed-loop system. The cable pulley system is attached in the same plane as the constriction beam on the actuator as shown in Fig. 5.

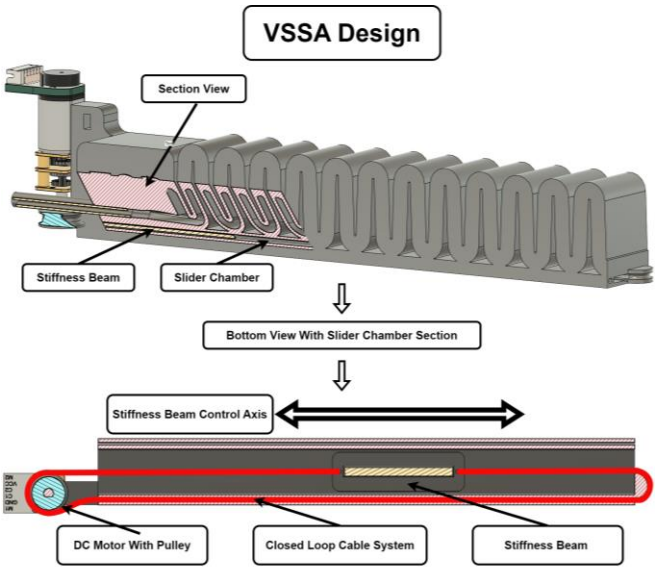

Figure 5. VSSA design with closed-loop stiffness beam actuation.

Additionally, the fabrication process of the VSSA was also considered during the design phase. The Fused Deposition Modeling (FDM) additive manufacturing technology used to fabricate the design operates in a layer-by-layer nature. The thickness of the top surface during the printing process is kept 0.4 mm thicker than the thickness of the bottom (standard 1.2 mm thick). This ensures a proper application of the top 3D printed layers as the first 2 top layers act as a mesh on which the remaining top layers are supported as there are no internal support structures in the geometry of the design.

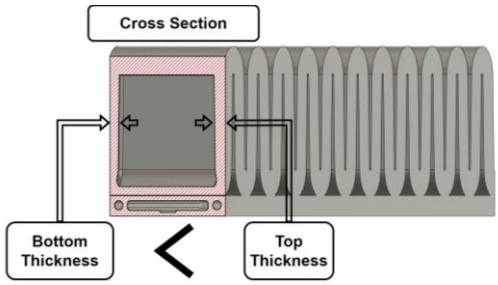

Figure 6: VSSA manufacturing wall thickness difference between top and bottom surfaces.

III. Simulations, Experiments, and Results

Testing the performance of the capabilities of the VSSA required a comparison between the experimental data against Finite Element Analysis (FEA) simulations. A mathematical model of the pneumatic soft actuator is a complex item to produce, therefore, FEA simulations are used for validating the experimental data of the performance of the design. In this section, the focus is on the formulation and development of a comprehensive finite element model. The goal is to create a sophisticated computational tool capable of accurately predicting the mechanical behavior and, more specifically, the bending performance of the pneumatic actuator. This entails a detailed exploration of the underlying simulation parameters involved in capturing the intricate dynamics of the actuator under varying conditions. The significance of such a model lies in its potential to provide valuable insights into the actuator's response to pneumatic pressurization, enabling a deeper understanding of its mechanical output. The developed finite element model serves as a valuable analytical tool for researchers and engineers seeking to optimize and fine-tune the design parameters of pneumatic actuators for enhanced bending performance [25]. The simulations and experiments were performed on four different configurations of the VSSA. The initial configuration (Config 0) placed the stiffness beam out of the deforming section of the VSSA. The next 3 configurations placed the stiffness beam in the slider chamber such that a third of the deformation section of the VSSA was constricted successively for each configuration as shown in Fig. 7. The stiffness beam position for each configuration between 1 and 3 is selected as they roughly correspond with the joint-blocking orthosis alternative rehabilitation therapies as shown in Fig. 1.

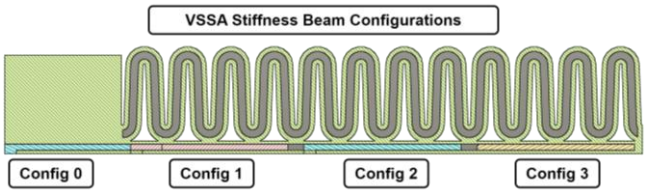

Figure 7. VSSA stiffness beam configurations.

A. Simulation

The simulation of the VSSA design was performed using FEA Static Structure Analysis in the Ansys Workbench. Ansys provides a powerful platform for conducting complex simulations of hyper-elastic material with a high degree of control over the simulation parameters. To enable a higher chance of convergence in the simulations, the VSSA design was simplified for the simulations. The internal chamfers and differences in wall thickness were removed as those items assisted in the manufacturing process of FDM 3D printing only. The tube features used for guiding the control cable of the stiffness beam were also removed as they were not used during the simulations.

The material model of the hyper-elastic material was added to the simulation engineering data with the Mooney-Rivlin model as discussed above in the material section. Specific model geometry was selected into named selections for the model to make contact selections easier. The geometry contacts were then enabled between all surfaces that were predicted to come in contact. The contacts were set as

"Frictionless" contacts between all surfaces of the VSSA model. Additionally, in order to hold the position of the stiffness beam at a constant location within the slider chamber, a small extruded surface on the stiffness beam was attached to the slider chamber using the "Bonded" contact. The deforming sections of the VSSA were set as fixed surfaces. The sections were set as grounded supports and were used as reference points in comparison to the remaining deforming surfaces. The surfaces of the internal chambers of the VSSA were selected to exert a constant pressure perpendicular to the internal surfaces with a ramped pressure from 0 to 23 kPa. Additionally, the side surfaces of the VSSA were applied with a displacement constraint which allowed the simulation to only deform in two degrees of freedom (DoF). The constraint was added to assist the convergence of the solution and assisted in the initial deformation phase of the simulations of the VSSA. Fig. 8 below shows the simulation setup of the VSSA.

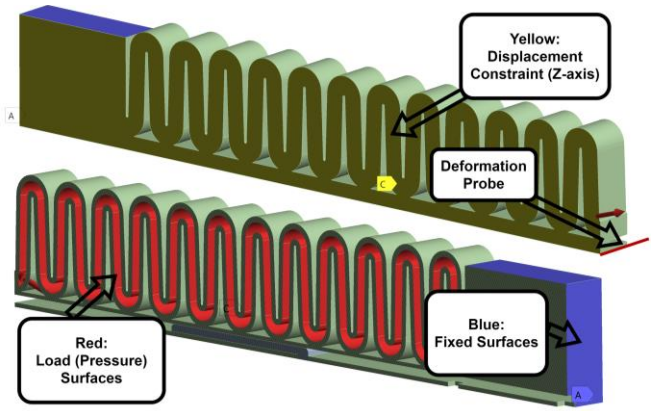

Figure 8. FEA simulation setup of the VSSA.

The expected outcome of the simulation was non-linear as the properties of the hyper-elastic material follow the Mooney-Rivlin second order model. The mesh settings were set to non-linear mechanical mesh with quadratic elements [26]. The average size of the mesh elements throughout the VSSA model was set to 1.5 mm. Due to the high bending contact nature of the stiffness beam and the sliding chamber, an increased mesh density was required in the slider chamber region containing the stiffness beam to achieve proper convergence of the solution. The contact sizing feature in the Ansys mesh controls was used to increase the mesh density in the stiffness region by reducing the mesh element size to 0.7 mm. The whole VSSA design was not set to such a high mesh density to reduce computational load during the simulations. Fig. 9 illustrates the increased mesh density feature in more detail.

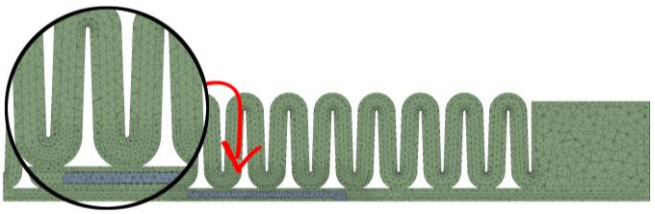

Figure 9. FEA simulation mesh with refined contact mesh.

Lastly, the analysis settings for the simulations were configured. The simulation was set to a one-second time with the initial step starting at 0.001 s. The small initial step size was set to allow the solution to reach convergence more gradually as it ramped the pressure to the final value. The minimum step size was set to 0.0005 s which assisted the simulation in overcoming challenges during contact change phases in the VSSA and the maximum step size was kept at the default setting of 1 s. Additionally, the solver was configured to an iterative solver for the simulation and large deflections were enabled.

Once all the simulation settings were configured, the simulation was run using a total deformation analysis with two deformation probes attached to the end tip of the VSSA as shown in Fig. 8 The deformation in the *X* and *Y* axes was measured with respect to the original un-deformed model of the simulation. The results in Fig. 10 show the simulations conducted in Ansys for each of the configurations with convergence time plots.

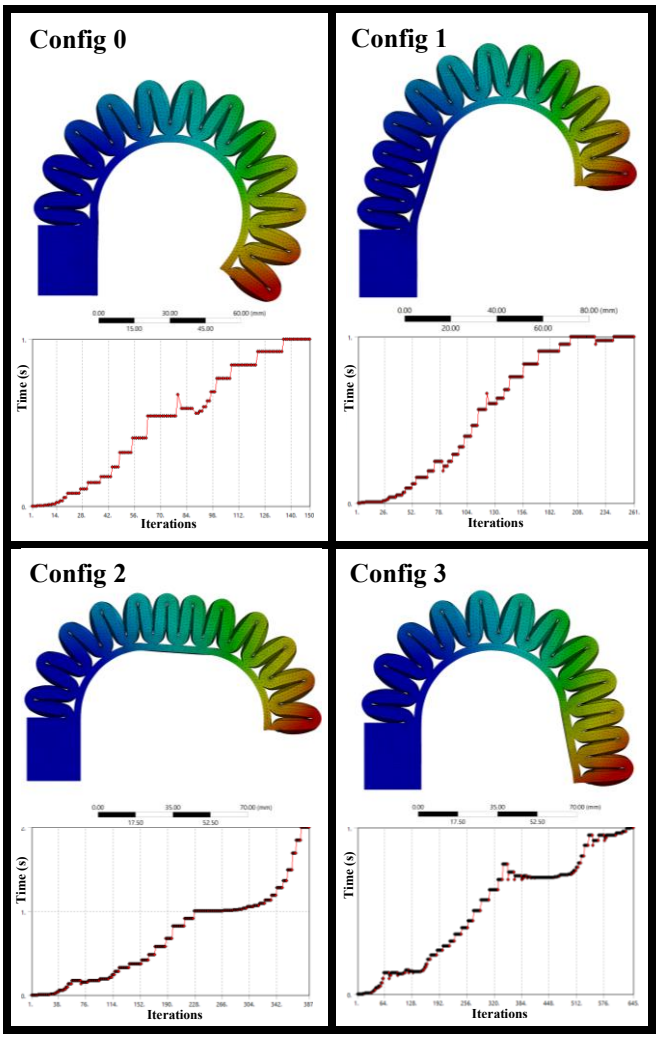

Figure 10. VSSA FEA simulation results.

B. *Experiment*

The experiments were conducted using the same approach as the FEA simulations. The VSSA was fixed to a board from the non-deforming surfaces at the base of the actuator. Air was supplied through a high-pressure and high-flow source with a regulator at the source to limit the amount of airflow and pressure in the VSSA. The air pressure was also monitored using a high-accuracy pressure sensor with a measurement

range of 0 to 400 kPa. After flowing through the pressure sensor, the air was channeled through a polyurethane tube to the actuator. The experimental setup described follows the diagram as shown in Fig. 11 below.

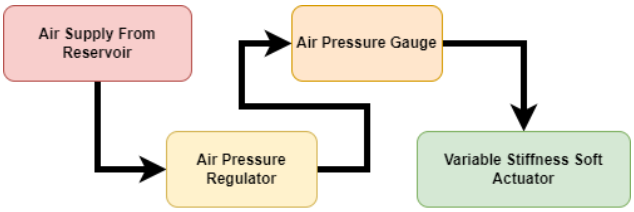

Figure 11. VSSA Experimental setup

The small DC motor on the VSSA was used to control the position of the stiffness beam in the slider chamber. The four different configurations were individually set for each experiment. The pressure in the VSSA was ramped using a valve on the regulator from 0 to 120 kPA as measured on the pressure gauge. The cause of the pressure difference between the FEA simulations and experiments of the VSSA is discussed further in the comparison section below. The pressure was ramped for each configuration from 0 to 30, 40, 60, 80, 100, and 120 kPa consecutively. The deformation of the VSSA in each configuration was observed using a camera mounted at a fixed position above the deforming VSSA. The camera was used to capture the deformation of the VSSA at each pressure point mentioned above between 0 and 120 kPa. The figure below shows the final deformation achieved by the VSSA in each configuration.

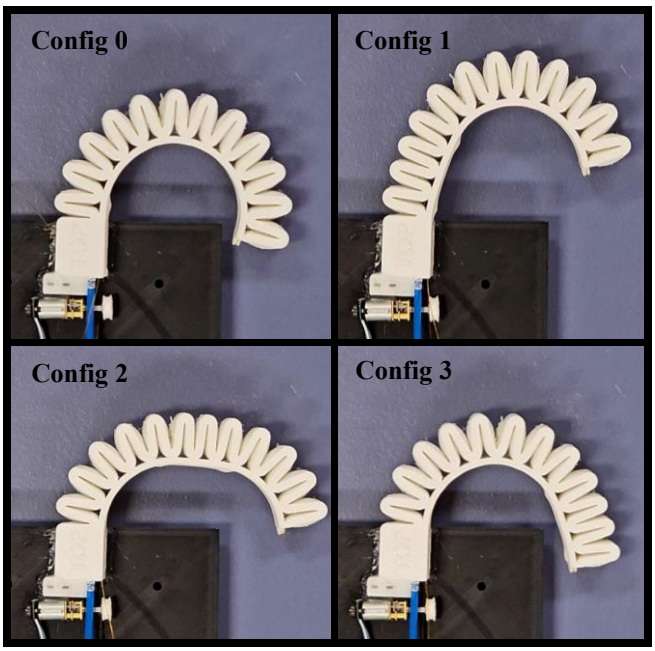

Figure 12. VSSA Experimental results

C. *Comparison*

Upon completion of the experiments, the VSSA tip deformation trajectory of the FEA simulations was compared against the experimental data. The tip deformation was noted as per the position of the probe in Fig. 8 and was used in both scenarios. The data was directly retrieved from the Ansys results for the FEA simulation and raw displacement measurements were used for the experimental data. The images for the experiment were scaled appropriately and used to measure the deformation of the VSSA. The deformation measurements were taken from the bottom right corner of the VSSA to the actuator tip, which is the same point as the probe in the simulation.

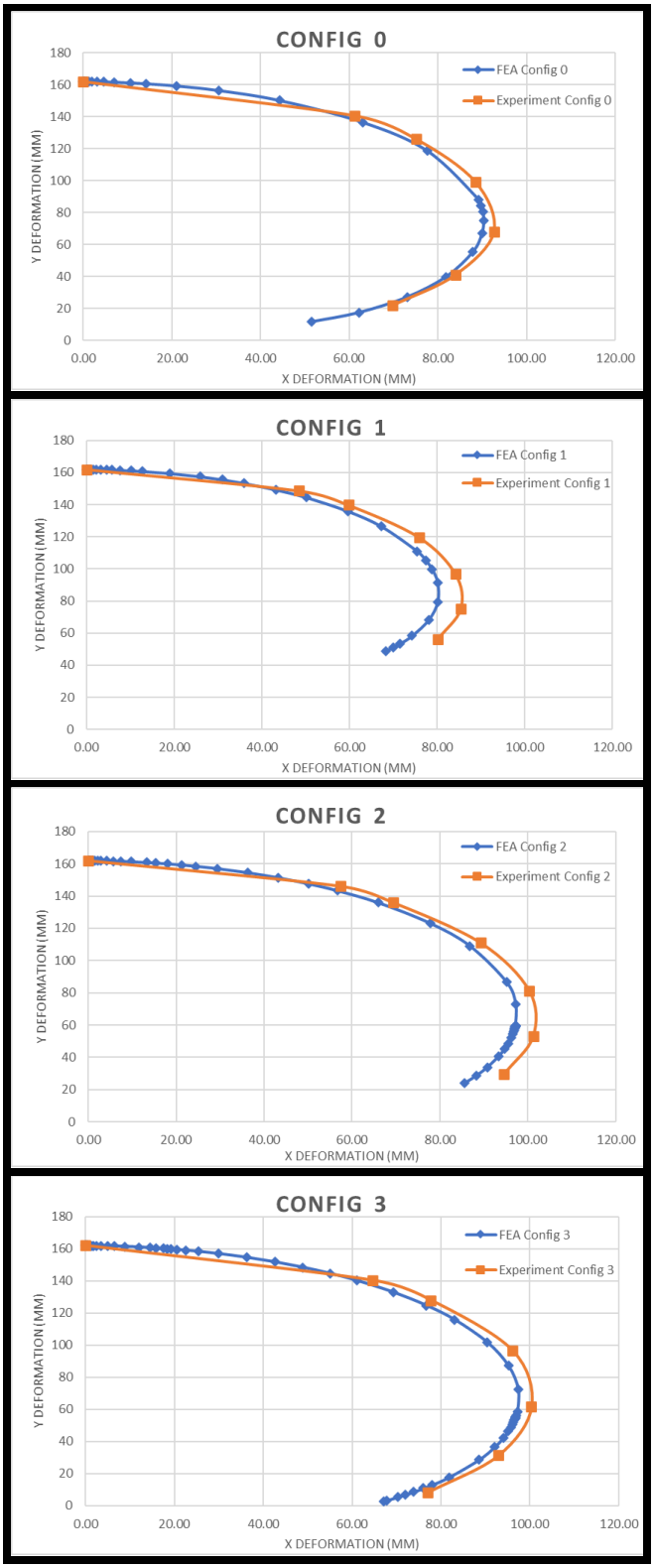

Figure 13. VSSA Experimental and FEA simulation tip deformation comparison

The analysis of the tip deformation plots of the VSSA shows that despite the difference in required pressure, both the FEA simulations and experiments follow a very similar trajectory with slight variations in the X-axis deformation. Table II below displays a comparison of the X-axis deformation between the two sets of data for each configuration, showcasing the maximum difference in the deformation of the VSSA being 5.37 mm on configuration 1 with a percentage difference of only 6.49%. The Y-axis deformation was not compared as the difference in pressure required for the deformation was not modeled. Due to the lack of a reliable model for the air leak, the plots in all configurations show that the overall deformation in the FEA simulations was greater than in the experiments on the Y-axis.

TABLE II. FEA vs Experiment Maximum X-Axis Deformation

VSSA Config	FEA vs Experiment X-Axis Deformation			
	FEA Max (mm)	Experiment Max (mm)	Max Difference (mm)	% Difference
Config 0	90.34	92.66	2.32	2.50
Config 1	80.05	85.42	5.37	6.49
Config 2	97.26	101.26	4.00	4.03
Config 3	97.36	100.33	2.98	3.00

Furthermore, the change in stiffness of the actuator on the X-axis was determined by comparing the deformation of all the configurations with respect to config 0. The change in stiffness along the Y-axis was not calculated due to the lack of the deformation model caused by the air leaks. The stiffness change of the actuator was calculated as a function of the actuation pressure and the X-axis deformation. Table III below shows the result of the calculated values. Config 1 shows the greatest change in stiffness in the X-axis at the given actuation pressure of 120 kPa with a stiffness variation of 12% at the equilibrium position when compared against config 0. The data also indicates that config 2 and config 3 have negative values, indicating the stiffness has been decreased resulting from a larger X-axis deformation. However, an important item to note is that the results shown are only within the X-axis and do not wholistically represent the system. The results show that change in stiffness of specific regions with the VSSA have been achieved as a result of manipulating the position of the stiffness beam within the slider chamber of the actuator.

TABLE III. Change in VSSA Stiffness on the X-axis

VSSA Config	Actuation Pressure (kPa)	Deformation (mm)	Stiffness k (N/m^3)	% Change in Stiffness
Config 0	120	92.66	1295	0.0
Config 1	120	85.42	1405	12.0
Config 2	120	101.26	1185	-8.5
Config 3	120	100.33	1200	-7.3

IV. Challenges

Manufacturing errors caused by the soft hyper-elastic material during the 3D printing process caused defects in the parameters of the expansion chambers of the actuator. The defects in the expansion chamber were the primary source of the air leaks. The air leaks across the VSSA expansion chambers were non-linear. Due to the irregularities in the defects present in the parameters of the expansion chambers in the VSSA, the air leaks vary across different configurations as the configuration changes (moving the stiffness beam), the expansion chambers in the stiff region deform less than those in the flexible region. Future iterations of the VSSA fabrication will use more robust manufacturing processes to ensure minimum air leaks with additional improvements in the design such as increasing wall thickness or using materials with more predictable printing characteristics.

The existing prototype lacks a feedback system, notably the absence of sensing elements. The integration of a feedback system is deemed essential for achieving precision in control. To enhance the device's responsiveness to external stimuli, the incorporation of diverse sensors becomes imperative. These sensors include but are not limited to, pressure sensors that measure the internal pressure of the expansion chambers, a soft elastic angle sensor that can be used in conjunction with the position of the stiffness beam to determine the final position of the actuator, and a force sensor to determine the power of the actuator [27]. This augmentation aims to fortify the device's robustness by providing real-time data on various parameters, enabling more accurate control and adaptability to dynamic environmental conditions.

V. Conclusion

In conclusion, an effective design of a soft variable stiffness actuator was proposed to perform alternative methods of hand rehabilitation therapies. The proposed design is capable of selectively modifying the stiffness of regions above desired joints, thus enabling a variety of different motions from a simple actuation source and a smaller actuator used for determining the stiffness of regions within the actuator. The proposed design was tested with four different configurations in which stiffness regions within the actuator are adjusted. The design was initially tested in a Finite Element Analysis simulation using hyper-elastic non-linear material settings which were used to determine the expected behavior of the actuator in different configurations as the pressure was increased. The simulation results were then compared to experimental results following the same configuration setup. Though the actuation pressure required was vastly different between the simulations and experiments due to air leaks, the actuator design demonstrated an acceptable replication of the FEA simulations with only minor differences in the tip trajectory of the actuator. Currently, only a single prototype has been tested to validate the design of a new form of variable stiffness actuator. Future work includes addressing the air leak issue through more robust manufacturing processes and building a fully functional hand rehabilitation glove capable of performing and testing the effectiveness of the alternative therapies proposed.

ACKNOWLEDGMENT

This work is supported by the National Science Foundation (NSF) grant under FRR-2131711.

REFERENCES

[1] S. Biggar and W. Yao, "Design and Evaluation of a Soft and Wearable Robotic Glove for Hand Rehabilitation," in IEEE Transactions on Neural Systems and Rehabilitation Engineering, vol. 24, no. 10, pp. 1071-1080, Oct. 2016, doi: 10.1109/TNSRE.2016.2521544.

[2] H. K. Yap, J. H. Lim, F. Nasrallah, J. Cho Hong Goh, and C.-H. Yeow, "Characterisation and evaluation of soft elastomeric actuators for hand assistive and rehabilitation applications," Journal of Medical Engineering & Technology, vol. 40, no. 4, pp. 199–209, Mar. 2016. doi:10.3109/03091902.2016.1161853.

[3] A. Stilli *et al*., "AirExGlove — A novel pneumatic exoskeleton glove for adaptive hand rehabilitation in post-stroke patients," *2018 IEEE International Conference on Soft Robotics (RoboSoft)*, Livorno, Italy, 2018, pp. 579-584, doi: 10.1109/ROBOSOFT.2018.8405388.

[4] K. H. L. Heung, R. K. Y. Tong, A. T. H. Lau, and Z. Li, "Robotic glove with soft-elastic composite actuators for assisting activities of Daily Living," *Soft Robotics*, vol. 6, no. 2, pp. 289–304, Apr. 2019. doi:10.1089/soro.2017.0125.

[5] R. Kabir, M. Sunny, H. Ahmed, and M. Rahman, "Hand rehabilitation devices: A comprehensive systematic review," Micromachines, vol. 13, no. 7, p. 1033, Jun. 2022. doi:10.3390/mi13071033

[6] W. Thimabut, P. Terachinda, and W. Kitisomprayoonkul, "Effectiveness of a soft robotic glove to assist hand function in stroke patients: A cross-sectional pilot study," *Rehabilitation Research and Practice*, vol. 2022, pp. 1–8, Apr. 2022. doi:10.1155/2022/3738219.

[7] N. Friedman *et al.*, "Retraining and assessing hand movement after stroke using the MusicGlove: Comparison with conventional hand therapy and isometric grip training," *Journal of NeuroEngineering and Rehabilitation*, vol. 11, no. 1, p. 76, 2014. doi:10.1186/1743-0003-11-76.

[8] S. H. Teo, D. C. Ng, and Y. K. Wong, "Effectiveness of proximal interphalangeal joint–blocking orthosis vs metacarpophalangeal joint–blocking orthosis in trigger digit management: A randomized clinical trial," *Journal of Hand Therapy*, vol. 32, no. 4, pp. 444–451, Oct. 2019. doi:10.1016/j.jht.2018.02.007.

[9] C.-H. Yeow, A. T. Baisch, S. G. Talbot, and C. J. Walsh, "Cable-driven finger exercise device with extension return springs for recreating standard therapy exercises," *Journal of Medical Devices*, vol. 8, no. 1, Dec. 2013. doi:10.1115/1.4025449.

[10] H. K. Yap, Jeong Hoon Lim, F. Nasrallah, J. C. H. Goh and R. C. H. Yeow, "A soft exoskeleton for hand assistive and rehabilitation application using pneumatic actuators with variable stiffness," *2015 IEEE International Conference on Robotics and Automation (ICRA)*, Seattle, WA, USA, 2015, pp. 4967-4972, doi: 10.1109/ICRA.2015.7139889.

[11] X. Li, Y. Hao, J. Zhang, C. Wang, D. Li and J. Zhang, "Design, Modeling and Experiments of a Variable Stiffness Soft Robotic Glove for Stroke Patients With Clenched Fist Deformity," in *IEEE Robotics and Automation Letters*, vol. 8, no. 7, pp. 4044-4051, July 2023, doi: 10.1109/LRA.2023.3279613.

[12] Soliman, AM, Hussain, I, Awad, MI, & Gan, D. "Design and Modeling of a Variable Stiffness Barrel Mechanism for Ankle Exoskeleton." *Proceedings of the ASME 2020 International Design Engineering Technical Conferences and Computers and Information in Engineering Conference. Volume 10: 44th Mechanisms and Robotics Conference (MR)*. Virtual, Online. August 17–19, 2020. V010T10A071. ASME. https://doi.org/10.1115/DETC2020-22650.

[13] Yang C, Geng S, Walker I, et al. Geometric constraint-based modeling and analysis of a novel continuum robot with Shape Memory Alloy initiated variable stiffness. The International Journal of Robotics Research. 2020;39(14):1620-1634. doi:10.1177/0278364920913929.

[14] Hussain I, Al-Ketan O, Renda F, et al. Design and prototyping soft–rigid tendon-driven modular grippers using interpenetrating phase composites materials. The International Journal of Robotics Research. 2020;39(14):1635-1646. doi:10.1177/0278364920907697.

[15] Fu, J.; Lin, H.; Prathyush, I.V.S.; Huang, X.; Zheng, L.; Gan, D. A Novel Discrete Variable Stiffness Gripper Based on the Fin Ray Effect. In Proceedings of the International Conference on Intelligent Robotics and Applications, Yantai, China, 22–25 October 2022; pp. 791–802. https://link.springer.com/chapter/10.1007/978-3-031-13835-5_71.

[16] Gao, Y., Huang, X., Mann, I. S., and Su, H. (June 5, 2020). "A Novel Variable Stiffness Compliant Robotic Gripper Based on Layer Jamming." ASME. *J. Mechanisms Robotics*. October 2020; 12(5): 051013. https://doi.org/10.1115/1.4047156.

[17] H. Godaba, A. Sajad, N. Patel, K. Althoefer and K. Zhang, "A Two-Fingered Robot Gripper with Variable Stiffness Flexure Hinges Based on Shape Morphing," *2020 IEEE/RSJ International Conference on Intelligent Robots and Systems (IROS)*, Las Vegas, NV, USA, 2020, pp. 8716-8721, doi: 10.1109/IROS45743.2020.9341554.

[18] Fu J, Yu Z, Guo Q, Zheng L, Gan D. A variable stiffness robotic gripper based on parallel beam with vision-based force sensing for flexible grasping. Robotica. Published online 2023:1-19. doi:10.1017/S026357472300156X.

[19] D. Gonzalez, J. Garcia, R. M. Voyles, R. A. Nawrocki, and B. Newell, "Characterization of 3D printed pneumatic soft actuator," *Sensors and Actuators A: Physical*, vol. 334, p. 113337, Feb. 2022. doi:10.1016/j.sna.2021.113337.

[20] M. Lalegani Dezaki, M. Bodaghi, A. Serjouei, S. Afazov, and A. Zolfagharian, "Soft pneumatic actuators with controllable stiffness by bio-inspired lattice chambers and fused deposition modeling 3D printing," *Advanced Engineering Materials*, vol. 25, no. 6, Jan. 2023. doi:10.1002/adem.202200797.

[21] C. Dudescu and L. Racz, "Effects of raster orientation, infill rate and infill pattern on the mechanical properties of 3D printed materials," *ACTA Universitatis Cibiniensis*, vol. 69, no. 1, pp. 23–30, Dec. 2017. doi:10.1515/aucts-2017-0004.

[22] Recreus, "FILAFLEX 60A TECHNICAL DATA SHEET," datasheet, Mar. 2018 [Revised Mar. 2018].

[23] M. R. Sheikhi, B. Shamsadinlo, Ö. Ünver, and S. Gürgen, "Finite element analysis of different material models for polyurethane elastomer using estimation data sets," *Journal of the Brazilian Society of Mechanical Sciences and Engineering*, vol. 43, no. 12, Nov. 2021. doi:10.1007/s40430-021-03279-9.

[24] B. W. K. Ang and C. -H. Yeow, "Print-it-Yourself (PIY) glove: A fully 3D printed soft robotic hand rehabilitative and assistive exoskeleton for stroke patients," *2017 IEEE/RSJ International Conference on Intelligent Robots and Systems (IROS)*, Vancouver, BC, Canada, 2017, pp. 1219-1223, doi: 10.1109/IROS.2017.8202295.

[25] D. Quevedo-Moreno and E. T. Roche, "Design and Modeling of Fabric-Shelled Pneumatic Bending Soft Actuators," in *IEEE Robotics and Automation Letters*, vol. 8, no. 6, pp. 3110-3117, June 2023, doi: 10.1109/LRA.2023.3264734.

[26] P. Curkovic and A. Jambrecic, "Improving structural design of soft actuators using finite element method analysis," *Interdisciplinary Description of Complex Systems*, vol. 18, no. 4, pp. 490–500, 2020. doi:10.7906/indecs.18.4.8.

[27] D. M. Vogt, Y. -L. Park and R. J. Wood, "Design and Characterization of a Soft Multi-Axis Force Sensor Using Embedded Microfluidic Channels," in *IEEE Sensors Journal*, vol. 13, no. 10, pp. 4056-4064, Oct. 2013, doi: 10.1109/JSEN.2013.2272320.